Electronic Supplementary Material (ESI) for Physical Chemistry Chemical Physics.

SUPPLEMENTARY INFORMATION

Mechanism of powellite crystallite expansion within nano-phase separated amorphous matrices under Au-irradiation

Karishma B. Patel[a], Sophie Schuller[b], Giulio I. Lampronti[a], Ian Farnan[a]*

[a] Department of Earth Sciences, University of Cambridge, Downing Street, Cambridge, CB23EQ, UK

[b] CEA, DES, ISEC, DE2D, Université Montpellier, Marcoule, Bagnols-sur-Cèze, France

S1 TRIM calculations

The radiation experiment performed in this study was conducted at CSNSM using 7 MeV Au^{3+} ions. TRIM calculations were performed in order to estimate the ion penetration depth and therefore the irradiated volume, in addition to characteristics of displacement cascades. Figure S1 shows the ion ranges in the CNO substrate, summarising that the penetration depth is estimated to be ~1.5 μm. Figure S2 shows the ionisation energy attributed to both ions and recoil atoms. This is an important factor as it was used to explain temperature-like effects on crystallisation kinetics following irradiation.

Figure S1 – S6 show various results from TRIM calculations for irradiation of CNO. Similar results in terms of the ion ranges were found for other compositions (± 0.2 μm), hence why only the output values for a single calculation are provided here.

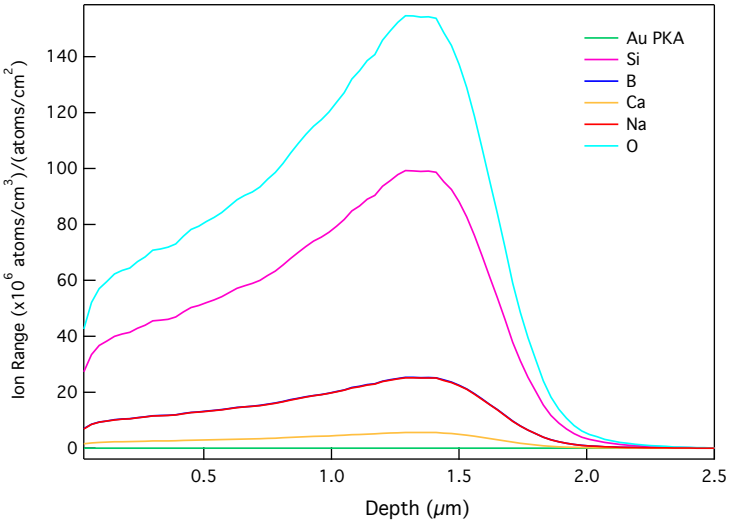

Figure S1: Ion ranges with the CNO substrate, indicating a penetration depth of 1.6 μm.

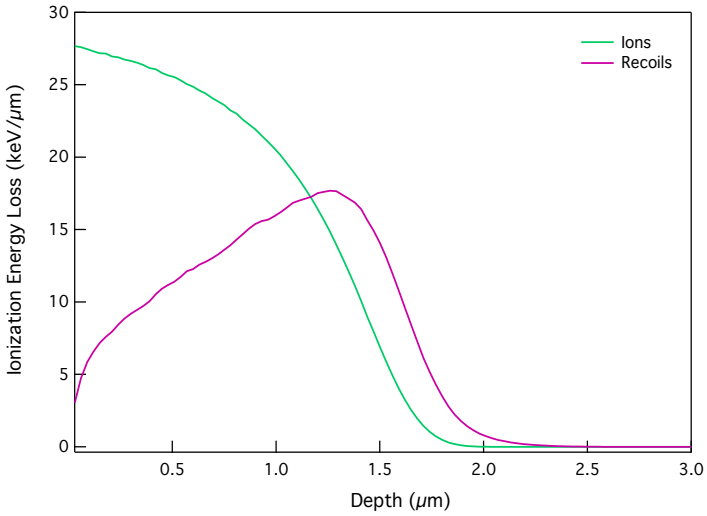

Figure S2: Electronic and nuclear stopping power of Au^{3+} as a function of energy

Figure S3 shows the electronic and nuclear energy loss (stopping power) as a function of the ion energy, while Figure S4 shows the target replacement collisions resulting from an atomic displacement where an incoming atom gets trapped in the site of the same species of atom following collision. Although the collision is taking place, the configuration of the glass can sometimes remain the same if it is replaced by another atom of the same species. This could be a contributing factor to the limited modifications viewed in glasses. The corresponding deposited energy for each

component can be seen in Figure S5, which subsequently creates the vacancies trajectories seen in Figure S6.

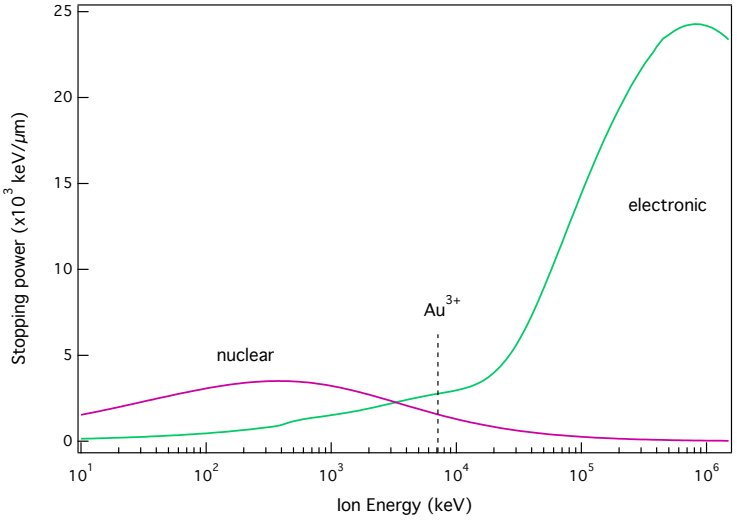

Figure S3: Electronic and nuclear stopping power of Au^{3+} as a function of energy

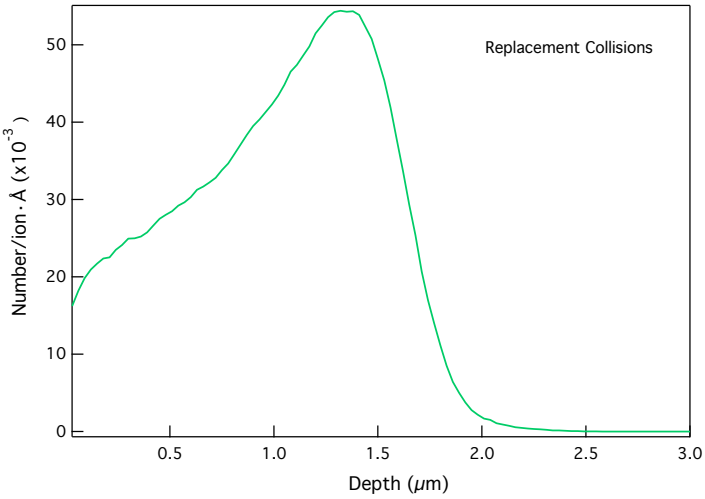

Figure S4: Ionisation energy attributed to ion (green) and recoils nuclei (pink).

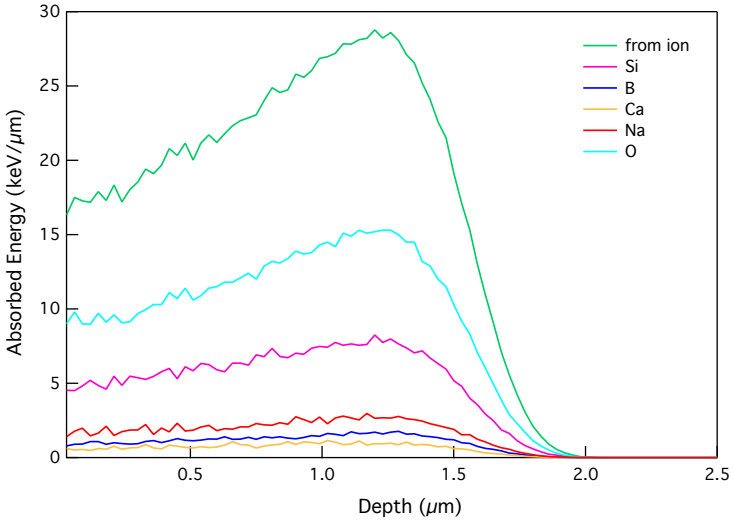

Figure S5: Absorbed energy from ions (green) to specified atoms: Si (pink), B (blue), Ca (orange), Na (red), O (light blue)

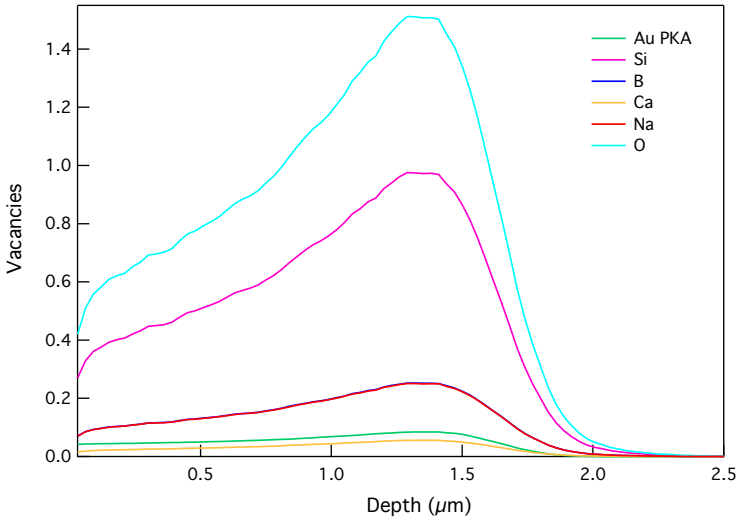

Figure S6: Vacancies created for Si (pink), B (blue), Ca (orange), Na (red) O (light blue) from primary knock-on atoms (PKA) Au ions.

S2 SDT spectrum

Thermal analysis reported the presence of two glass transition temperatures (T_g) and a melting temperature (T_M) of $CaMoO_4$, or an analogous Ca-Mo amorphous phase. These findings were summarised in the main text based on SDT spectra, an example of which can be seen in Figure S7.

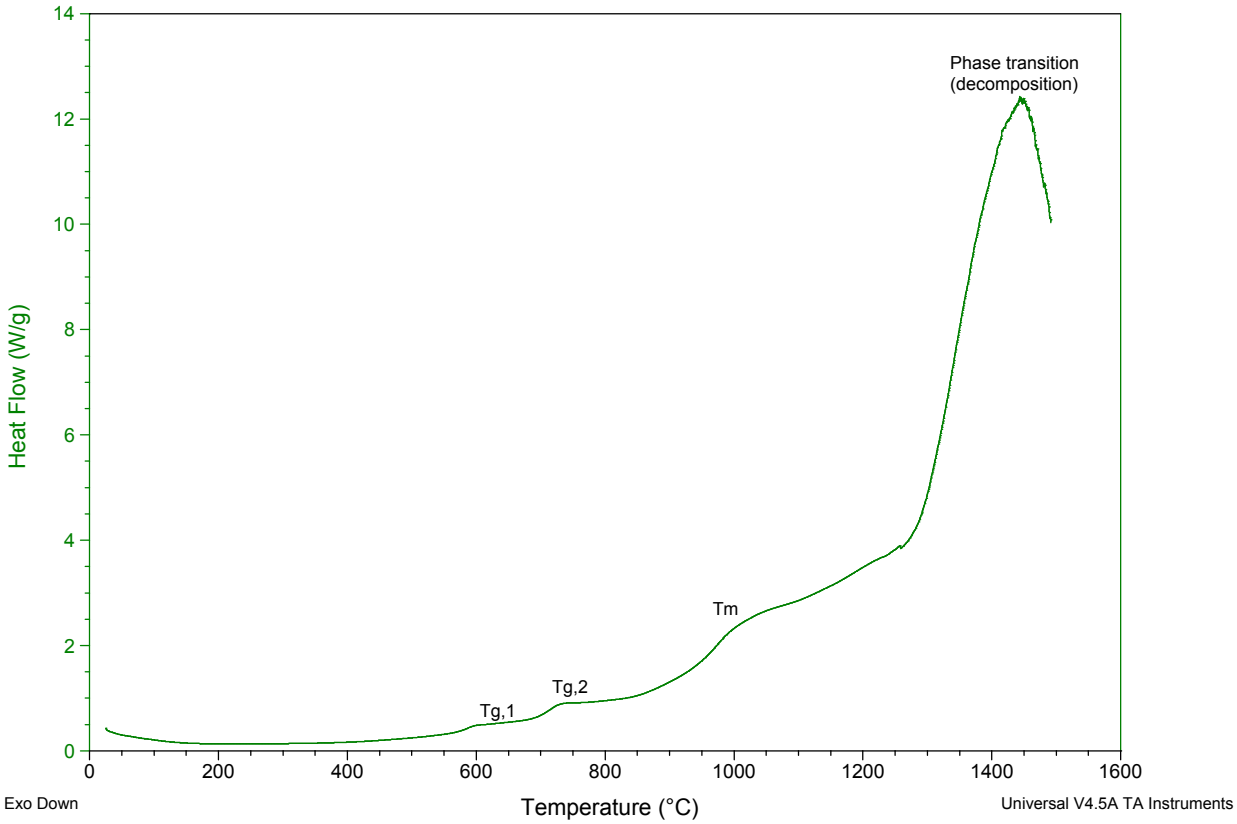

Figure S7: SDT spectra of amorphous CNG1 from Universal V4.5A TA Instruments software. The spectrum illustrates two glass transitions, the melting temperature of powellite, and the onset of decomposition or volatilisation of boron.

S3 SEM micrographs of amorphous samples

The retention limit of MoO_3 and sample classification of glass versus GC were determined both by XRD and SEM BSE. While it is assumed that no $CaMoO_4$ occurred for $[MoO_3] \leq$ 1mol%, this glass as well as CNO exhibited multiple glass transitions indicative of phase separation. The micrographs in Figure S8 indicate that micro-scale phase separation has not occurred, but granulation in the imaging could be representative of spinodal decomposition occurring on the nano-scale.

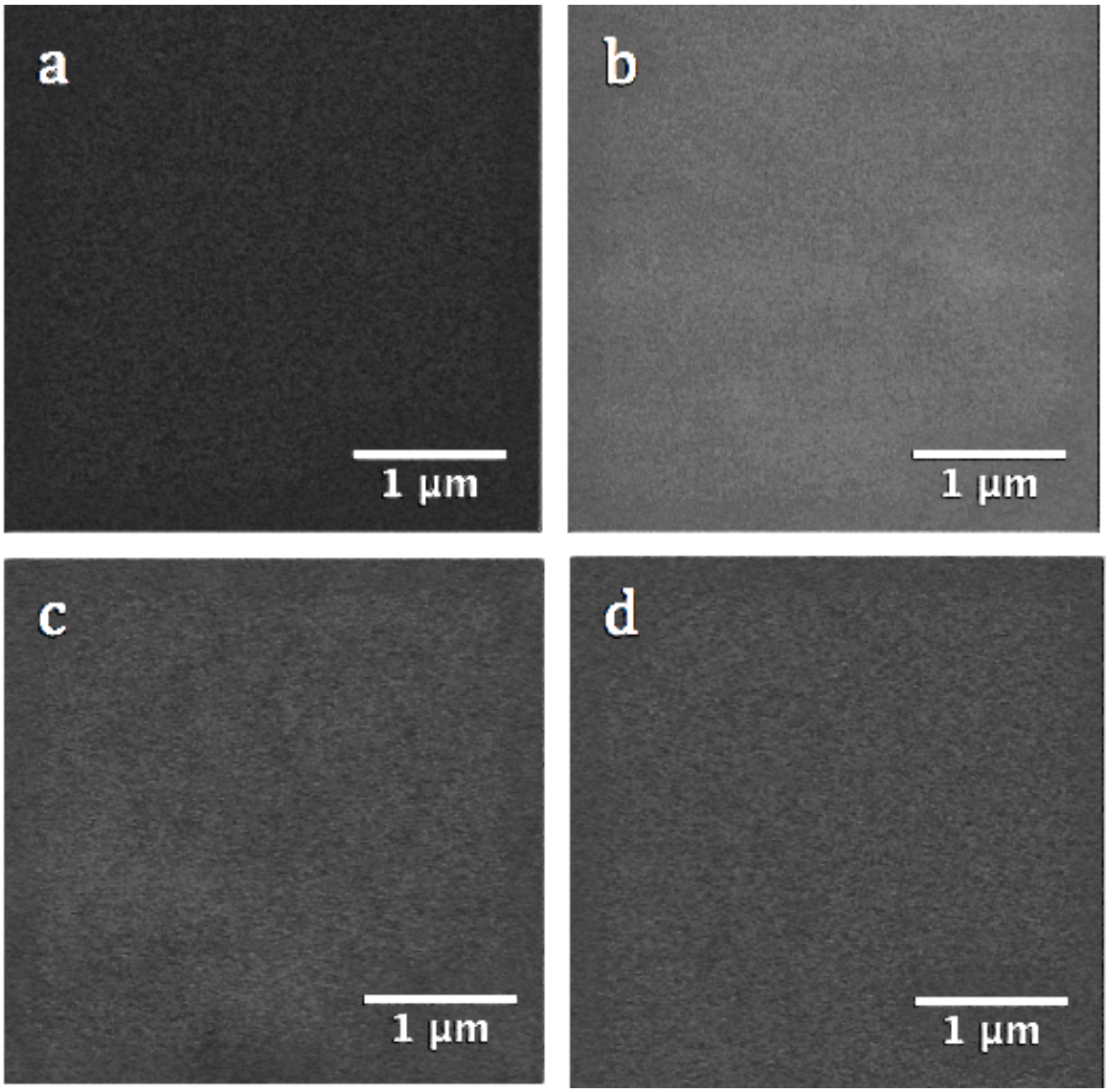

Figure S8: BSE micrographs of CNO: a) following synthesis, and b) following Au-irradiation; and of CNG1: c) following synthesis, and d) following Au-irradiation.

S4 XRD patterns

In this paper Scherrer crystallite size (CS) valuations were determined from structural analysis based on whole pattern Rietveld refinements with the software Topas v4.1 [1]. The results of this analysis are presented in the main body of the text, and are based on the spectra seen in Figure S9. CNG1 is clearly amorphous and all diffraction peaks in CNG1.75, CNG2.5, CNG7 and CN10 are assigned to $CaMoO_4$. Similar patterns are observed following irradiation with various changes to intensity and linewidth, thus presenting changes to CS and the lattice parameters.

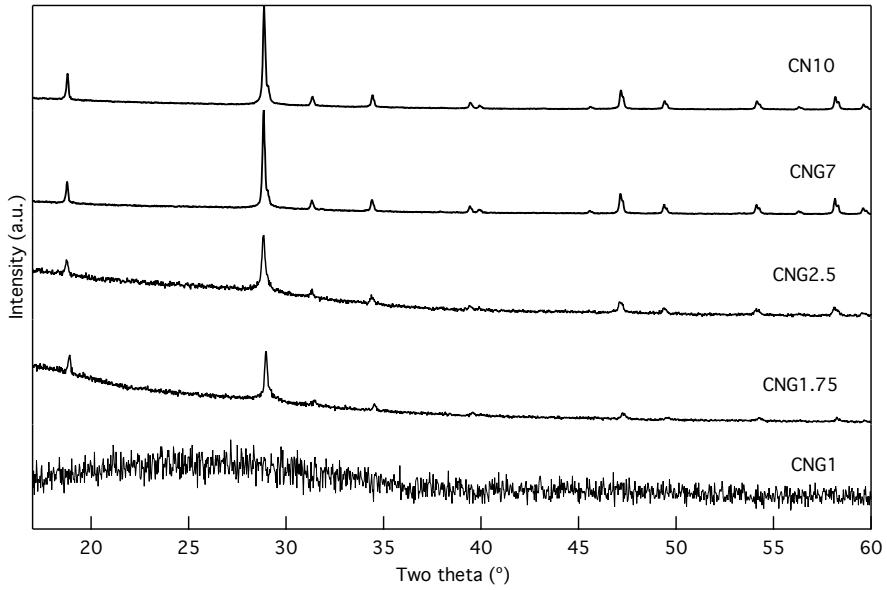

Figure S9: Raw XRD patters of pristine samples with increasing [MoO_3].

REFERENCES

(1) Cheary, R. W.; Coelho, A. a.; Cline, J. P. Fundamental Parameters Line Profile Fitting in Laboratory Diffractometers. *J. Res. Natl. Inst. Stand. Technol.* **2004**, *109* (1), 1–25. https://doi.org/10.6028/jres.109.002.

S5 Additional Raman analysis

As mentioned in the text, Raman spectroscopy was used to confirm the homogeneity of amorphous samples CNO, and CNG1. In each of these samples, three to five randomly selected points across the surface were chosen for analysis. As the spectral shape remained constant for each of the three samples at pristine conditions (see Figure S10 for an example), it can be concluded that these compositions are macroscopically homogeneous in the distribution of network formers. Therefore, phase separation indicated by SDT results must be occurring periodically on a scale smaller than the 2 μm spot size used for Raman analysis.

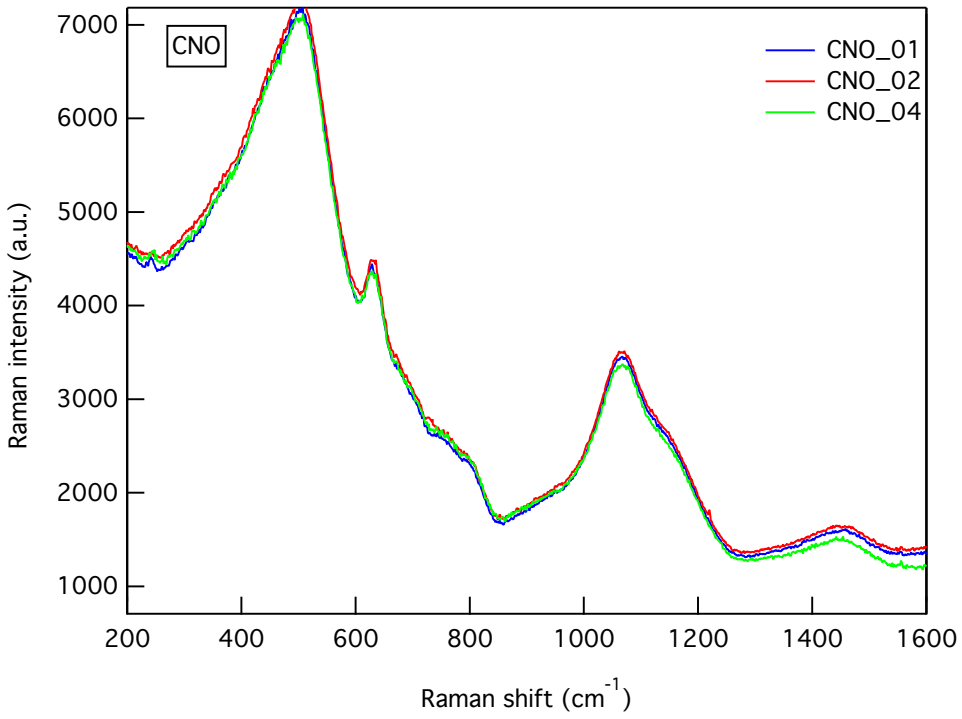

Figure S10: Raman spectra from multiple measurements across the sample surface of pristine CNO. The spectral shape similarity between randomly selected spots indicates homogeneity in this amorphous composition.